Self-similarity, density-size dynamics and the sinking speed of marine aggregates.

Andre W. Visser[1], **Anton Vergod Almgren**[1]

[1]VKR Centre for Ocean Life, National Institute of Aquatic Resources, Technical University of Denmark, Kongens Lyngby, Denmark

Key Points:

- Poor estimates of the sinking speed of marine aggregates stem primarily high variance in aggregate excess density.
- Self-similarity of aggregation facilitates efficiently modelling of aggregate size and excess density, and hence sinking speed.
- This provides a mechanistic description of how planktonic communities impact the size and density-resolved export flux of organic matter.

Corresponding author: A.W. Visser, `awv@aqua.dtu.dk`

Abstract

We propose self-similarity of aggregation provides a tractable framework for estimating the sinking speed of natural marine particle aggregates for ocean biogeochemical models. It does so by providing a means to tracking both size and excess density of aggregates as they are formed and transformed by aggregation, degradation and fragmentation processes. A self-similarity parameter a in the range 1.8 to 2.1 is well supported by direct observations drawn from an extensive database of aggregate size and sinking speed. This provides a mechanistic description of how spatial and temporal variations in planktonic communities impact size and density characteristic of aggregate assemblages and their subsequent export from the surface ocean. We provide a simple model for which we conduct sensitivity analyses for the self-similarity parameter, stickiness, and turbulent dissipation rate. While incomplete in several aspects, the model compares well with observations of aggregate size spectra covering the global ocean.

Plain Language Summary

How fast dead stuff sinks is perhaps the biggest uncertainty in estimating how the world's oceans cycle elements, and in particular, how they sequester carbon. We present a model that links surface plankton communities with the density and size characteristics of the aggregates of dead material they produce, and are thus able to estimate the sinking speeds of all aggregates that emerge. A key assumption that allows for efficient simulation is self-similarity of aggregation; that the underlying process of how aggregates form is well described by a set of global rules, even though this is often hidden by differences in what they are made of, and how they are degraded and fragmented. Although really quite simple, our model compares well with macroscopic properties of aggregates assemblages seen in nature.

1 Introduction

Perhaps the greatest hurdle to attaining a mechanistic understanding of the oceans' biogeochemical cycles is the incomplete description of the sinking speeds of particulate matter. This issue is central to key questions such as how much organic material is exported from the sunlit surface ocean (Ducklow et al., 2001; Mouw et al., 2016), its dependence on the ever changing structure of the surface plankton community (Boyd & Newton, 1995; Henson et al., 2012), the depth to which detrital material sinks before being solubilized (Cavan et al., 2017; Marsay et al., 2015), what this means for carbon sequestration (Kwon et al., 2009), consumption of oxygen (Suess, 1980; Bopp et al., 2002) nutrient recycling (Tréguer & Jacques, 1992; Buesseler et al., 2007), and how much reaches the seabed to be buried in sediments or feed benthic communities (Gooday, 2002; Cael, Bisson, et al., 2021). Despite years of observations from laboratory and field, sinking speeds of natural aggregate particles remain as enigmatic as ever; aggregates of any size from microns to centimeters seemingly sink at any speeds from practically zero to several 1000s of meters per day (Iversen & Lampitt, 2020; Laurenceau-Cornec et al., 2020; Cael, Cavan, & Britten, 2021). Yet the physics of sinking speed is unequivocal. Sinking speed is set by a balance between buoyancy forces and drag (Stokes, 1851; Clift et al., 1978), and while the precise formulation may not be as neat as Stokes' law (Oseen, 1910; White, 1991; Loth, 2008), the following principle must hold: sinking speed is a monotonically increasing function of aggregate size and excess density *ceteris paribus*.

The key concept we explore here is that aggregation is a geometrically self-similar process, such that the linear dimension $r_{i\circ j}$ of an aggregate formed by the combination of two parent aggregates of linear dimension r_i and r_j respectively is given by:

$$r_{i\circ j} = (r_i^a + r_j^a)^{(1/a)} \tag{1}$$

That is, for the binary process of aggregation, r^a is an additive conservative property. This is not a new idea (Jackson, 1998; Wiesner, 1992) and arises from the general observation that aggregates are fractal objects (Alldredge & Gotschalk, 1988; Meakin, 1987; Logan & Wilkinson, 1990). We term a the self-similarity parameter, and note $a < 3$ in compliance with the observed increase in porosity under aggregation. We stress that a is not the fractal dimension of the aggregate. Neither is it an inherent property of aggregates and we will not attempt to use a to produce scaling laws as is the usual trajectory of these considerations. At this point we simply want to treat a as a parameter governing the binary process of aggregation.

Under geometric self-similarity, the total mass of an aggregate produced by the combination of 2 aggregates of mass m_i and m_j can be deduced to be the sum of these two masses, plus a bit extra due to the inclusion of some fluid (density ρ_w) that occupies the expanded aggregate volume (i.e. increase in porosity). Specifically,

$$m_{ioj} = m_i + m_j + (v_{ioj} - v_i - v_j)\rho_w \tag{2}$$

where v_i, v_j and v_{ioj} are the volumes of the two parent aggregates and the daughter aggregate respectively. Note that m is the total mass, not just the dry mass of the aggregate. It is convenient to recast this in terms of density of the aggregates, ρ_i, ρ_j, ρ_{ioj}. It follows that excess density

$$\rho_{ioj} - \rho_w = \frac{r_i^3}{r_{ioj}^3}(\rho_i - \rho_w) + \frac{r_j^3}{r_{ioj}^3}(\rho_j - \rho_w) \tag{3}$$

Equations (1) and (3) provide a construct by which the size and excess density, and hence sinking speed, of particle aggregates can be estimated. However, processes other than aggregation also effect size and density; chief amongst these are degradation, dissolution and fragmentation. This is illustrated in Figure 1 for a single primary particle (a diatom for instance) where aggregation produces larger and less dense aggregates, degradation and /or dissolution removes mass but has no immediate impact on aggregate size, and fragmentation, particularly on large porous aggregates produces smaller aggregates which can be reincorporated into the aggregation process. Though out, sinking speed can be estimated. At the system scale (*e.g.* the surface mixed layer), a dynamic can be established between the supply of primary particles (*e.g.* from primary production, deposition of dust, faecal pellets) and the loss of aggregates by sinking. While still relatively complex, each of the sub-processes can in principle be constrained from observations, parameterized and mechanistically formulated. What makes this framework particularly attractive is the development of size-based and trait-based models of plankton communities (Banas, 2011; Serra-Pompei et al., 2020; Serra-Pompei et al., 2022) which provide precisely the type of information (size and trait resolved primary productivity and zooplankton grazers) that can serve as input. Indeed a resolved particle aggregation model can provide a mechanistic link between emerging plankton community structure and export flux; one of the key unresolved issues of the biological carbon pump (Boyd & Newton, 1995; Bach et al., 2019).

2 Analysis of self-similarity from observations.

A large literature exists reporting observations of the sinking speed and size of marine aggregates. These were recently collated and published in a database (Laurenceau-Cornec et al., 2015; Cael, Cavan, & Britten, 2021), and, together with additional observations (Gärdes et al., 2011; Bach et al., 2019; Iversen & Lampitt, 2020) provide the basis for this analysis. While aggregate density in itself is a difficult parameter to measure, it can be estimated from observed sinking speeds (Engel et al., 2009; Iversen & Ploug, 2010). In particular,

$$\rho - \rho_w = \frac{3}{8}\frac{Cw^2}{gr} \tag{4}$$

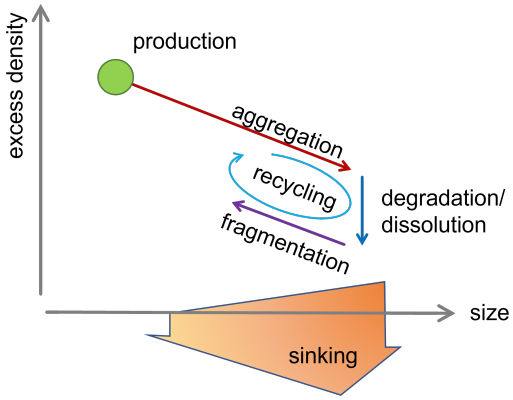

Figure 1. Aggregate dynamics depicted in 2 dimensional state space. Dynamics are driven by 3 processes; aggregation producing larger less dense aggregates, degradation/dissolution which reduces the solid mass (and hence excess density) of aggregates, and fragmentation. Primary particles (e.g. diatoms) are produce in a specific size and density range. The production of other material such as dust and TEP can also be specified. The distribution of aggregates in this state space eventually reaches steady state when the rate of supply is balanced by the sinking losses particularly of large dense aggregates.

where w is sinking speed, r the estimated spherical radius, g the gravitational acceleration, and C is an empirically derived drag coefficient. While there are several formulations, generally expressed as a function of Reynolds number ($R = 2rw/\eta$, with η being the kinematic viscosity of seawater), the most commonly used is

$$C = \frac{24}{R} + \frac{6}{1+\sqrt{R}} + 0.4 \tag{5}$$

(White, 1991). This, and similar formulas are robust for R up to about 10^5. Estimates of excess density and observed sinking speed for aggregates are plotted in Figure 2 and summarized in Table 1. The preponderance of observations correspond to $R < 100$ and thus lie well within the range where (5) is valid. The general features of Figure 2 neatly illustrate some of the properties of aggregation already mentioned. For instance, that large aggregates tend to sink faster and have a lower excess density than small aggregates. Further, while there is considerable variance of sinking speed with size, this appears to be reduced for excess density. Indeed, the ensemble of excess density observations appears to collapse roughly to a power law r^b with b around -1.4.

Under special conditions, self-similarity makes quite strong predictions on how aggregate properties (e.g. mass, density, porosity) scale with size. Specifically, for a monoculture of primary particles of size r_0 and density ρ_0, and in the absence of degradation, dissolution, and fragmentation, then aggregates' excess density follows a power law:

$$\rho(r) - \rho_w = (\rho_o - \rho_w)\left(\frac{r}{r_0}\right)^{a-3} \tag{6}$$

Under these conditions, the aggregation vector in the Figure 1, would have an expected slope $a - 3$.

Within the set of field and laboratory observations reported in Table 1, a subset meet suitable criteria that can reveal such a relationship. For instance, (Iversen & Ploug, 2010) conducted laboratory studies of aggregates from relatively fresh monocultures of the chain forming diatom *Skeletonema costatum* and the coccolithophore *Emiliania huxleyi*, and mixtures of the two. Log-log regressions on these indicate b in the range -1.2

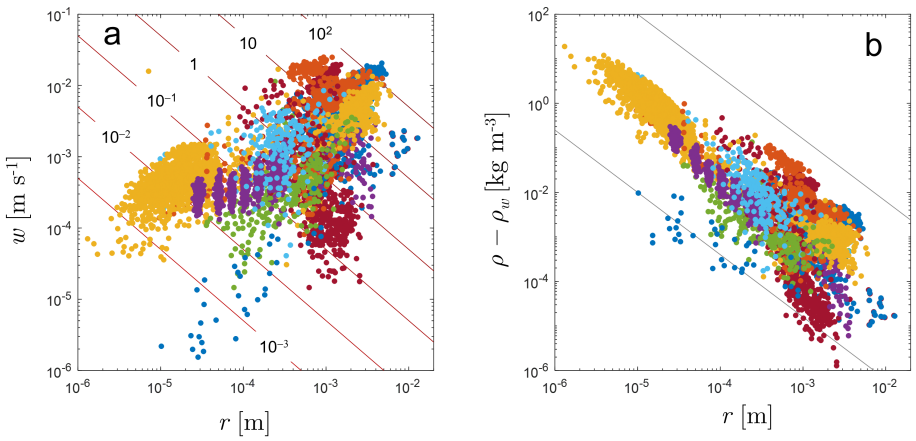

Figure 2. (a) Aggregate sinking speed (w) observed in a large number of studies (cf. Table 1) as a function of estimated spherical radius (r) and (b) the excess density ($\rho - \rho_w$) calculated from observed sinking speeds using a modified Stokes law. Colors represent different studies. The lines in panel (a) are contours of Reynolds number ranging from 100 to 0.001. The grey lines in panel (b) indicate a log-log slope of -1.4.

to -1.0 i.e. a in the range 1.8 to 2.0. Other laboratory observations that have avoided degradation and extraneous manipulations with TEP and dust indicate similar relationships with b in the range $[-1.2, -0.9]$ (Engel & Schartau, 1999; Engel et al., 2009; Laurenceau-Cornec et al., 2015). These values are consistent with laboratory experiments for non-biological particle aggregation (Lin et al., 1989) for which a ranges between 1.8 and 2.1. The lower value corresponds to a relatively porous structure that arises when aggregates are built-up of very sticky, similarly sized particles that combine immediately on contact. The value $a = 2$ corresponds to a random walk arrangement in 3 dimensions, and has been used in previous model settings (Jackson & Burd, 1998; Jokulsdottir & Archer, 2016). From these considerations, it appears that a in the ranges 1.8 to 2.1 is a reasonable choice.

It is also clear that a large number, indeed the majority, of studies listed in Table 1, exhibit slopes b that are spread across a much broader range. These studies all follow quite different experimental (e.g. natural aggregates, lab cultures, manipulations with ballast material) and observational procedures (e.g. *in situ* cameras, roller tanks, vertical flow systems). In some instances it can be argued that the observation method is poorly designed to capture the characteristics of the full aggregate community. Roller tanks for instance preferentially generate large, fast-sinking aggregates (Jackson, 2015) producing particle size spectra that are not representative of natural aggregate communities. Perhaps more important is the heterogeneity of the primary particles. In some experimental setups, ballasting material of considerably different excess densities are present or introduced. Further, natural plankton communities are seldom mono-cultures, and are generally composed of unicellular organisms covering a range of sizes and densities; some with shells and spines, some vacuolated, some chain-forming. In any given size range, the aggregate community will be an ad-mixture derived from different primary particles. Furthermore, as aggregates degrade and fragment, smaller, less dense aggregates come into the mix – grist to the mill – so that aggregate density, and hence sinking speed, will exhibit a relatively broad distribution at any given aggregate size. We must therefore conclude that while the majority of observations plotted in Figure 2 are perfectly fine in relating the sinking speed to the size of an aggregate, methodological issues mean that

they remain mute on any self-similarity in the underlying aggregation process. Seen in this light, it appears that the variance of excess density (Figure 2 (b)) is composed of two elements; a general negative slope being due to increased aggregate porosity with size, and an inherent variability due to the excess density of primary aggregate material.

3 Dynamic Aggregate Model

Here we provide a brief description of a simplified model . The physical setting we consider is a surface mixed layer of depth h where aggregates are produced from a range of primary particles, transformed and sink out according to the dynamics described in Figure 1. The model simulates the number and mass of aggregates in a two dimensional state space (size and excess density). We supply the code for the model in the supplementary material, and encourage readers to perform their own simulations.

It is convenient right from the outset to introduce two transformed variable (x, z) that map to $(r, \rho - \rho_w)$ as

$$r = r_o \delta^x, \quad \rho - \rho_w = \rho_o z \delta^{(a-3)x} \tag{7}$$

x is a logarithmic scaling of aggregate size, and z a stretched linear scaling of excess density. The factor $\delta^{(a-3)x}$ takes advantage of the reduction of density by aggregation and expands the density resolution for large aggregates. Key variables in the model are the matrices N and M representing the number of aggregates and their total mass respectively within 1×1 bins in discretized (x, z) state space. Suitable range choices for x and z, scaling factors r_o [µm] and ρ_o [kg m^{-1}], and logarithmic interval δ allow for a relatively complete representation of the aggregate community within computationally convenient dimensions of N and M. These are related by $\mathsf{M} = \mathsf{m} \circ \mathsf{N}$ where $\circ$ represents piece-wise matrix product and m is the mean mass of an aggregate within each bin.

The model determines the rate of change of M due to five processes: production, aggregation, degradation, fragmentation and sinking losses. Several of these processes are relatively simple to implement. For instance production is prescribed and sinking losses $\mathsf{Q} = -\mathsf{M} \circ \mathsf{w}/h$, where w is the mean aggregate sinking speed in discretized state space. Aggregation is computationally the most complex aspect of the model as it involves a binary convolution of N (Smoluchowski, 1916). It is governed by encounter kernels β; the rate at which aggregates collide, and stickiness α; the probability that collision will lead to aggregation (Burd & Jackson, 2009; Jokulsdottir & Archer, 2016). Performing binary convolution calculations is greatly facilitated by self-similarity. Specifically, the ordinates of an aggregate produced from the combination of (x_i, z_i) and (x_j, z_j) is given by:

$$\begin{aligned} x_{i\circ j} &= x_i + \log_\delta((1 + \delta^{(x_j - x_i)a}))/a \\ &= x_j + \log_\delta((1 + \delta^{(x_i - x_j)a}))/a \\ z_{i\circ j} &= \frac{z_i}{1 + \delta^{(x_j - x_i)a}} + \frac{z_j}{1 + \delta^{(x_i - x_j)a}}. \end{aligned} \tag{8}$$

It follows that the combination of aggregates from any two 1×1 bins in state space will be confined to a third 1×1 bin, albeit offset from the matrix grid spacing. The model utilizes this in optimizing the algorithm architecture.

We implement degradation as a drift of particle numbers to lower density bins. Specifically, if γ is the degradation rate, then it can be shown that the z ordinate of an aggregate follows $dz/dt = -\gamma z$. In this, degradation acts only on excess density. We set $\gamma = 0.1$ day^{-1} consistent with a range of studies (Kiørboe, 2001; Cavan & Boyd, 2018; Bach et al., 2019) although it should be noted that there is considerable variation. Finally fragmentation is simulated simply as a rate at which aggregate mass is transported to smaller

sizes classes. We implement this as an increasing function of aggregate size. Of the processes considered, fragmentation remains the least well constrained; aggregates appear resistant to mechanical shear (Alldredge et al., 1990), and fragmented appears to be chiefly mediated by metazooans through handling and feeding appears to be important (Dilling & Alldredge, 2000) and by microbial "mining" and dissolution of adhesive material. We set the maximum fragmentation rate at 0.5 day^{-1} for large porous aggregates, a value consistent with observations (Briggs et al., 2020).

4 Results and sensitivity

We present a series of simulations for a fixed rate of primary particle production (size range 1 to 30 µm in radius, excess density range 10 to 100 kg m^{-3}) that corresponds to a mixed community of unicellular auto- and heterotrophic plankton ranging from cyanobacteria to diatoms. Simulations were run to quasi-steady state (i.e. relative differences between successive daily estimates (normalized root-mean-square deviation) were $< 10^{-6}$) using a MATLAB ode solver. Three sets of parameters (self-similarity, stickiness and turbulent dissipation rate) were varied between runs and the emerging aggregate community was characterized by its size spectrum and size resolved export flux. All simulations assumed a mixed layer depth of $h = 50$ m, and a production rate of $P_{\text{total}} = 0.1$ gC m^{-2} day^{-1} of primary detrital particles. Results are presented in Figure 3, and the numerical code that produced it can be found in the supplementary material.

Particle size spectra $n(r(x)) = \sum_z \mathsf{N}(x,z)/dr(x)$ were estimated in the normal manner (Burd & Jackson, 2009) as per size bin width and provide a macroscopic measure of the underlying dynamics of production, transformation and sinking. Measurements of such spectra are routinely made and often conform to a power law of the form $n(r) \sim r^p$. Observations (Stemmann et al., 2008; Guidi et al., 2009; Reynolds & Stramski, 2021) from different oceanic regions and spanning aggregate sizes from microns to centimeters, show that p ranges from -2 to -6 and cluster around -3 to -4 in the surface ocean. For our model simulations (Figure 3:b,d,f), all runs exhibited particle size spectra slopes of about -4 for aggregates from 1 to several 100s of µm in size.

The flux distributions $f(r(x)) = \sum_z \mathsf{M}(x,z) \circ \mathsf{w}(x,z)/(hP_{\text{total}})$ are the flux contributions summed over different excess density bins, reported within aggregate size bins and normalized with regards total primary particle production P_{total}. The net sum is a little less than unity; difference being due to the net loss of mass due to degradation. The shape of $f(r)$ is universally dome-shaped with very little flux at either small (low sinking speed) or large (low total mass) aggregate sizes. The peak of the flux distribution, and to some extent its width, varies with self-similarity, stickiness and turbulent dissipation rate. Low self-similarity indices for instance, push the flux distribution towards larger aggregate sizes, as do high turbulent dissipation rates. Stickiness by contrast has a relatively minor influence on the flux distribution. Maximum flux appears to be associated with a steepening of the particle size spectrum $n(r)$.

While we have argued that a universal self-similarity index, if it exists, is relatively well constrained within the range $[1.8, 2.1]$, this range still presents a large variation in the characteristics of the export flux. For instance, the peak of the flux distribution (Figure 3 a) ranges over an order of magnitude in aggregate size, from 300 to 3000 µm. Further, the flux distribution range is much narrower for high self-similarity indices, a feature that is exacerbated given the logarithmic scaling of the size bins. The total export flux however, remains virtually the same across all these self similarity values (within 99% of each other). Indeed, the self similarity parameter has counteracting effects on sinking speed in terms of aggregate size and excess density (large a produce small but low porous aggregates and vice versa). The sinking speeds for aggregates in flux maxima (Figure 3 a) vary only modestly, from 10 to 20 m day^{-1} across all values of the self-similarity parameter. It should be noted that the export flux distribution in terms of aggregate size,

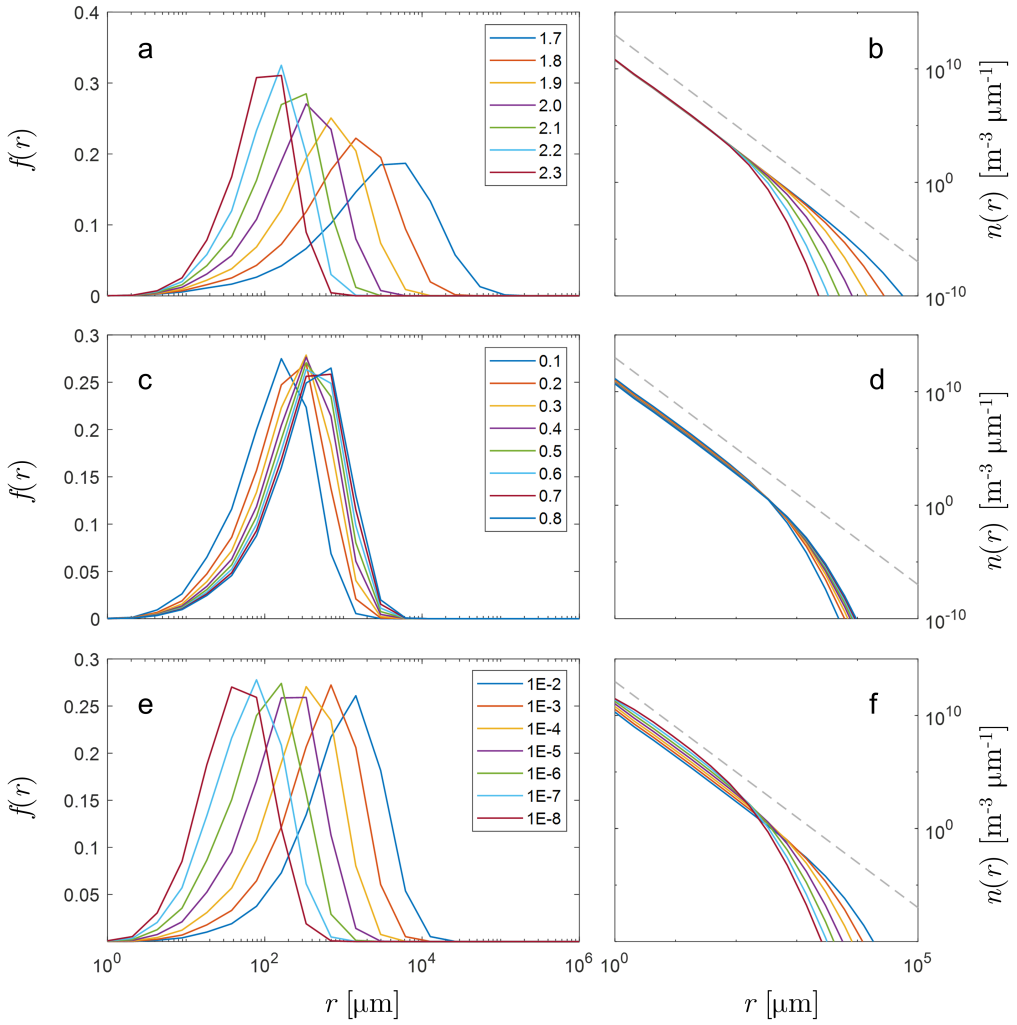

Figure 3. Aggregate community structure at steady state; $f(r)$ size resolved normalized export flux (a,c,b) and $n(r)$ particle size spectra (b,d,f) for a range of different a self-similarity parameters (a,b), α stickiness coefficients (c,d) and turbulent dissipation rates [m^2 s^{-3}] (e,f). Dissipation rates are related to encounter rate β as given in (Burd & Jackson, 2009). Dashed lines in (b,d,f) indicate log-log slopes of -4.

excess density and sinking speed sets many of the key characteristics of the subsequent flux attenuation curve within the mesopelagic (e.g. remineralization length scale (Cavan et al., 2017) and subsequent sequestration time scales (Boyd et al., 2019)). While we cannot at this time provide argumentation to further constrain the self-similarity parameter, we have put in place a mechanistic model that can guide empirical studies to improve resolution.

5 Conclusions

Much of the literature concerning the fractal dimensions of aggregates has been built on the restrictive assumptions of irreversibity and uniform primary particles (Meakin, 1987; Lin et al., 1989) which leads to the rather handy definition that the fractal dimension of aggregates a' can be found from their mass-size relationship $m \sim r^{a'}$ (Meakin, 1987; Burd & Jackson, 2009). At the same time, aggregates found in the marine environment have been deemed to be fractal objects in that they display fractal type properties (Alldredge & Gotschalk, 1989; Logan & Wilkinson, 1990); an increase in porosity and a decrease in excess density as a function of size for instance. There is however a disconnect between these two concepts, namely that aggregation in the marine environment is not irreversible; aggregates degrade and fragment, and they are not composed of identical primary particles. All manner of primary particles are introduced into the surface ocean by primary producers, sloppy feeding, fecal matter and aeolian dust deposits. Further, the constituent components of detritus vary significantly in excess density (relative to seawater $\rho_w = 1027$ kg m^{-3}) ranging from positively buoyant e.g. TEP in the range -200 to -300 kg m^{-3} (Azetsu-Scott & Passow, 2004) and lipids around -100 kg m^{-3} (Visser & Jónasdóttir, 1999) to near neutrally buoyant e.g. cytoplasm 3 to 70 kg m^{-3} (Tappan & Loeblich Jr, 1973) , to very much negatively buoyant, e.g. coccoliths 1700 to 1900 kg m^{-3} (Toktamış et al., 2016), diatom frustules 1600 kg m^{-3} (Miklasz & Denny, 2010) and atmospheric dust (quartz, feldspar, calcite) approximately 1700 kg m^{-3}. It is no surprise that neither a well constrained fractal dimension nor a size dependent sinking speed for marine aggregates has been found.

More than anything, the poor ability to estimate the sinking speed of marine aggregates stems from the high variability of their excess density. Other factors, like shape, surface roughness and the through flow of interstitial fluid have been suggested, but at most, contribute a factor 2 to sinking speed corrections. This is negligible compared to the orders of magnitude variance (yet alone a potential change in sign) exhibited in the excess density. The modelling framework we propose is designed specifically to track both size and excess density throughout an emerging aggregate community. We purposefully present the model itself in its simplest form. In this we are mindful that overly complex models become increasingly inscrutable, and unattractive for integration into higher level computational products. There are clearly aspects that can be expanded. For instance resolving aggregate porosity would allow a distinction between dry mass and total mass and provide a more robust implementation of degradation and fragmentation processes. Stickiness is also a parameter that shows large variability in primary material (from TEP to dust). Further, temporal aspects such as annual cycles of productivity, turbulence and mixed layer depth are yet to be explored. Finally, our concept of self-similarity of aggregation, and a governing parameter a constrained to the range 1.8 to 2.1 is certainly open to scrutiny, particularly given its impact on the emerging flux-size distribution. That there is some systematic control on aggregate size and density is evident in figure 2.b. How this is manifest in particular setting is however highly variable. We argue that in part, this variability can be accounted for through the aggregation process for which we provide a mechanistic description. A large part of the variance remains however, and reflects the vastly different excess densities of the primary material from which the aggregates derive. Failure to recognize the variability in the density of primary material and

how this propagates through an aggregate community confounds efforts to estimate fluxes and attenuation length scales of particulate matter in the oceans.

6 Open Research

The model code and associated documentation for the simulations presented here is open source, and freely available on GitHub github.com/AndyWVisser/Aggregation and zenodo.org/record/6731544#.Yra-0HZBxPY. Data sets used in the analysis are available in the supplementary material and accessible at zenodo.org/record/6731670#.Yra9i3ZBxPY.

Acknowledgments

This work was supported by the Centre for Ocean Life, a Villum Kann Rasmussen Centre of Excellence supported by the Villum Foundation, by the Gordon and Betty Moore Foundation (grant 5479), and has received funding from the European Union's Horizon 2020 research and innovation programme under grant agreement No 869383 (ECOTIP).

References

Alldredge, A. L., & Gotschalk, C. (1988). In situ settling behavior of marine snow. *Limnology and Oceanography*, *33*(3), 339–351. doi: 10.4319/lo.1988.33.3.0339

Alldredge, A. L., & Gotschalk, C. C. (1989). Direct observations of the mass flocculation of diatom blooms: characteristics, settling velocities and formation of diatom aggregates. *Deep Sea Research Part Ii: Topical Studies in Oceanography*, *36*, 159–171. doi: 10.1016/0198-0149(89)90131-3

Alldredge, A. L., Granata, T. C., Gotschalk, C. C., & Dickey, T. D. (1990). The physical strength of marine snow and its implications for particle disaggregation in the ocean. *Limnology and Oceanography*, *35*(7), 1415–1428.

Azetsu-Scott, K., & Johnson, B. D. (1992). Measuring physical characteristics of particles: A new method of simultaneous measurement for size, settling velocity and density of constituent matter. *Deep Sea Research Part A. Oceanographic Research Papers*, *39*(6), 1057–1066. doi: 10.1016/0198-0149(92)90039-v

Azetsu-Scott, K., & Passow, U. (2004). Ascending marine particles: Significance of transparent exopolymer particles (TEP) in the upper ocean. *Limnology and oceanography*, *49*(3), 741–748.

Bach, L. T., Stange, P., Taucher, J., Achterberg, E. P., Algueró-Muñiz, M., Horn, H., ... Riebesell, U. (2019). The influence of plankton community structure on sinking velocity and remineralization rate of marine aggregates. *Global Biogeochemical Cycles*, *33*(8), 971–994. doi: 10.1029/2019gb006256

Banas, N. S. (2011). Adding complex trophic interactions to a size-spectral plankton model: Emergent diversity patterns and limits on predictability. *Ecological Modelling*, *222*(15), 2663–2675. doi: 10.1016/j.ecolmodel.2011.05.018

Belcher, A., Iversen, M., Giering, S., Riou, V., Henson, S. A., Berline, L., ... Sanders, R. (2016). Depth-resolved particle-associated microbial respiration in the northeast Atlantic. *Biogeosciences*, *13*(17), 4927–4943. doi: 10.5194/bg-13-4927-2016

Bopp, L., Le Quéré, C., Heimann, M., Manning, A. C., & Monfray, P. (2002). Climate-induced oceanic oxygen fluxes: Implications for the contemporary carbon budget. *Global Biogeochemical Cycles*, *16*(2), 6–1. doi: 10.1029/2001gb001445

Boyd, P. W., Claustre, H., Levy, M., Siegel, D. A., & Weber, T. (2019). Multi-faceted particle pumps drive carbon sequestration in the ocean. *Nature*, *568*(7752), 327. doi: 10.1038/s41586-019-1098-2

Boyd, P. W., & Newton, P. (1995). Evidence of the potential influence of planktonic

community structure on the interannual variability of particulate organic carbon flux. *Deep Sea Research Part I: Oceanographic Research Papers*, *42*(5), 619–639. doi: 10.1016/0967-0637(95)00017-Z

Briggs, N., Dall'Olmo, G., & Claustre, H. (2020). Major role of particle fragmentation in regulating biological sequestration of CO2 by the oceans. *Science*, *367*(6479), 791–793.

Buesseler, K. O., Lamborg, C. H., Boyd, P. W., Lam, P. J., Trull, T. W., Bidigare, R. R., ... Wilson, S. (2007). Revisiting carbon flux through the ocean's twilight zone. *Science*, *316*(5824), 567–70. doi: 10.1126/science.1137959

Burd, A. B., & Jackson, G. A. (2009). Particle aggregation. *Annual Review of Marine Science*, *1*, 65–90. doi: 10.1146/annurev.marine.010908.163904

Cael, B. B., Bisson, K., Conte, M., Duret, M. T., Follett, C. L., Henson, S. A., ... Lampitt, R. S. (2021). Open ocean particle flux variability from surface to seafloor. *Geophysical Research Letters*, *48*(9), e2021GL092895. doi: 10.1029/2021gl092895

Cael, B. B., Cavan, E. L., & Britten, G. L. (2021). Reconciling the size-dependence of marine particle sinking speed. *Geophysical Research Letters*, *48*(5), e2020GL091771. doi: 10.1029/2020gl091771

Carder, K. L., Steward, R. G., & Betzer, P. R. (1982). In situ holographic measurements of the sizes and settling rates of oceanic particulates. *Journal of Geophysical Research: Oceans*, *87*(C8), 5681–5685. doi: 10.1029/jc087ic08p05681

Cavan, E. L., & Boyd, P. W. (2018). Effect of anthropogenic warming on microbial respiration and particulate organic carbon export rates in the sub-Antarctic Southern Ocean. *Aquatic Microbial Ecology*, *82*(2), 111–127.

Cavan, E. L., Trimmer, M., Shelley, F., & Sanders, R. (2017). Remineralization of particulate organic carbon in an ocean oxygen minimum zone. *Nature Communications*, *8*(1), 1–9.

Clift, R., Grace, J. R., & Webber, M. E. (1978). *Bubbles, Drops and Particles.* San Diego: Academic Press.

Diercks, A.-R., & Asper, V. L. (1997). In situ settling speeds of marine snow aggregates below the mixed layer: Black Sea and Gulf of Mexico. *Deep Sea Research Part I: Oceanographic Research Papers*, *44*(3), 385–398. doi: 10.1016/s0967-0637(96)00104-5

Dilling, L., & Alldredge, A. L. (2000). Fragmentation of marine snow by swimming macrozooplankton: A new process impacting carbon cycling in the sea. *Deep Sea Research Part I: Oceanographic Research Papers*, *47*(7), 1227–1245.

Ducklow, H. W., Steinberg, D. K., & Buesseler, K. O. (2001). Upper Ocean Carbon Export and the Biological Pump. *Oceanography*, *14*(4), 50–58. doi: 10.5670/oceanog.2001.06

Engel, A., Abramson, L., Szlosek, J., Liu, Z., Stewart, G., Hirschberg, D., & Lee, C. (2009). Investigating the effect of ballasting by CaCO3 in Emiliania huxleyi, II: Decomposition of particulate organic matter. *Deep Sea Research Part Ii: Topical Studies in Oceanography*, *56*(18), 1408–1419. doi: 10.1016/j.dsr2.2008.11.028

Engel, A., & Schartau, M. (1999). Influence of transparent exopolymer particles (TEP) on sinking velocity of Nitzschia closterium aggregates. *Marine Ecology Progress Series*, *182*, 69–76. doi: 10.3354/meps182069

Gibbs, R. J. (1985). Estuarine flocs: their size, settling velocity and density. *Journal of Geophysical Research: Oceans*, *90*(C2), 3249–3251. doi: 10.1029/jc090ic02p03249

Gooday, A. J. (2002). Biological responses to seasonally varying fluxes of organic matter to the ocean floor: a review. *Journal of Oceanography*, *58*(2), 305–332. doi: 10.1023/A:1015865826379

Guidi, L., Jackson, G. A., Stemmann, L., Miquel, J. C., Picheral, M., & Gorsky, G. (2008). Relationship between particle size distribution and flux in the

mesopelagic zone. *Deep Sea Research Part I: Oceanographic Research Papers*, *55*(10), 1364–1374. doi: 10.1016/j.dsr.2008.05.014

Guidi, L., Stemmann, L., Jackson, G. A., Ibanez, F., Claustre, H., Legendre, L., ... Gorskya, G. (2009). Effects of phytoplankton community on production, size, and export of large aggregates: A world-ocean analysis. *Limnology and Oceanography*, *54*(6), 1951–1963.

Gärdes, A., Iversen, M. H., Grossart, H.-P., Passow, U., & Ullrich, M. S. (2011). Diatom-associated bacteria are required for aggregation of Thalassiosira weissflogii. *ISME Journal*, *5*(3), 436–445. doi: 10.1038/ismej.2010.145

Henson, S., Lampitt, R., & Johns, D. (2012). Variability in phytoplankton community structure in response to the North Atlantic Oscillation and implications for organic carbon flux. *Limnology and Oceanography*, *57*(6), 1591–1601. doi: 10.4319/lo.2012.57.6.1591

Hill, P. S., Syvitski, J. P., Cowan, E. A., & Powell, R. D. (1998). In situ observations of floc settling velocities in Glacier Bay, Alaska. *Marine Geology*, *145*(1-2), 85–94. doi: 10.1016/s0025-3227(97)00109-6

Iversen, M. H., & Lampitt, R. S. (2020). Size does not matter after all: No evidence for a size-sinking relationship for marine snow. *Progress in Oceanography*, *189*, 102445. doi: 10.1016/j.pocean.2020.102445

Iversen, M. H., Nowald, N., Ploug, H., Jackson, G. A., & Fischer, G. (2010). High resolution profiles of vertical particulate organic matter export off Cape Blanc, Mauritania: Degradation processes and ballasting effects. *Deep Sea Research Part I: Oceanographic Research Papers*, *57*(6), 771–784. doi: 10.1016/j.dsr.2010.03.007

Iversen, M. H., & Ploug, H. (2010). Ballast minerals and the sinking carbon flux in the ocean: carbon-specific respiration rates and sinking velocity of marine snow aggregates. *Biogeosciences*, *7*(9), 2613–2624. doi: 10.5194/bg-7-2613-2010

Iversen, M. H., & Ploug, H. (2013). Temperature effects on carbon-specific respiration rate and sinking velocity of diatom aggregates–potential implications for deep ocean export processes. *Biogeosciences*, *10*(6), 4073–4085. doi: 10.5194/bg-10-4073-2013

Iversen, M. H., & Robert, M. L. (2015). Ballasting effects of smectite on aggregate formation and export from a natural plankton community. *Marine Chemistry*, *175*, 18–27. doi: 10.1016/j.marchem.2015.04.009

Jackson, G. A. (1998). Using fractal scaling and two-dimensional particle size spectra to calculate coagulation rates for heterogeneous systems. *Journal of Colloid and Interface Science*, *202*(1), 20–29. doi: 10.1006/jcis.1998.5435

Jackson, G. A. (2015). Coagulation in a rotating cylinder. *Limnology and Oceanography: Methods*, *13*(4), 194–201.

Jackson, G. A., & Burd, A. B. (1998). Aggregation in the marine environment. *Environmental Science & Technology*, *32*(19), 2805–2814. doi: 10.1021/es980251w

Jokulsdottir, T., & Archer, D. (2016). A stochastic, Lagrangian model of sinking biogenic aggregates in the ocean (SLAMS 1.0): model formulation, validation and sensitivity. *Geoscientific Model Development*, *9*(4), 1455–1476. doi: 10.5194/gmd-9-1455-2016

Jouandet, M.-P., Trull, T. W., Guidi, L., Picheral, M., Ebersbach, F., Stemmann, L., & Blain, S. (2011). Optical imaging of mesopelagic particles indicates deep carbon flux beneath a natural iron-fertilized bloom in the Southern Ocean. *Limnology and Oceanography*, *56*(3), 1130–1140. doi: 10.4319/lo.2011.56.3.1130

Kajihara, M. (1971). Settling velocity and porosity of large suspended particle. *Journal of the Oceanographical Society of Japan*, *27*(4), 158–162. doi: 10.1007/bf02109135

Kiørboe, T. (2001). Formation and fate of marine snow: small-scale processes with

large-scale implications. *Sci Mar*, *65*, 57–71.
Kwon, E. Y., Primeau, F., & Sarmiento, J. L. (2009). The impact of remineralization depth on the air–sea carbon balance. *Nature Geoscience*, *2*(9), 630–635. doi: 10.1038/ngeo612
Laurenceau-Cornec, E. C., Trull, T. W., Davies, D. M., De La Rocha, C. L., & Blain, S. (2015). Phytoplankton morphology controls on marine snow sinking velocity. *Marine Ecology Progress Series*, *520*(Buesseler 1998), 35–56. doi: 10.3354/meps11116
Laurenceau-Cornec, E. C., Le Moigne, F. A., Gallinari, M., Moriceau, B., Toullec, J., Iversen, M. H., ... De La Rocha, C. L. (2020). New guidelines for the application of Stokes' models to the sinking velocity of marine aggregates. *Limnology and Oceanography*, *65*(6), 1264–1285. doi: 10.1002/lno.11388
Lin, M., Lindsay, H., Weitz, D., Ball, R., Klein, R., & Meakin, P. (1989). Universality in colloid aggregation. *Nature*, *339*(6223), 360–362. doi: 10.1038/339360a0
Logan, B. E., & Wilkinson, D. B. (1990). Fractal geometry of marine snow and other biological aggregates. *Limnology and Oceanography*, *35*(1), 130–136. doi: 10.4319/lo.1990.35.1.0130
Loth, E. (2008). Drag of non-spherical solid particles of regular and irregular shape. *Powder Technology*, *182*(3), 342–353. doi: 10.1016/j.powtec.2007.06.001
Marsay, C. M., Sanders, R. J., Henson, S. A., Pabortsava, K., Achterberg, E. P., & Lampitt, R. S. (2015). Attenuation of sinking particulate organic carbon flux through the mesopelagic ocean. *Proceedings of the National Academy of Sciences*, *112*(4), 1089–1094. doi: 10.1073/pnas.1415311112
McDonnell, A. M., & Buesseler, K. O. (2010). Variability in the average sinking velocity of marine particles. *Limnology and Oceanography*, *55*(5), 2085–2096. doi: 10.4319/lo.2010.55.5.2085
Meakin, P. (1987). Fractal aggregates. *Advances in Colloid and Interface Science*, *28*, 249–331. doi: 10.1016/0001-8686(87)80016-7
Miklasz, K. A., & Denny, M. W. (2010). Diatom sinkings speeds: Improved predictions and insight from a modified Stokes' law. *Limnology and Oceanography*, *55*(6), 2513–2525.
Mouw, C. B., Barnett, A., McKinley, G. A., Gloege, L., & Pilcher, D. (2016). Phytoplankton size impact on export flux in the global ocean. *Global Biogeochemical Cycles*, *30*(10), 1542–1562. doi: 10.1002/2015gb005355
Nowald, N., Fischer, G., Ratmeyer, V., Iversen, M., Reuter, C., & Wefer, G. (2009). In-situ sinking speed measurements of marine snow aggregates acquired with a settling chamber mounted to the Cherokee ROV. In (pp. 1–6). IEEE. doi: 10.1109/oceanse.2009.5278186
Oseen, C. W. (1910). Uber die Stokes' sche Formel und Uber eine verwandte Aufgabe in der Hydrodynamik. *Arkiv Mat., Astron. Och Fysik*, *6*, 1.
Reynolds, R. A., & Stramski, D. (2021). Variability in oceanic particle size distributions and estimation of size class contributions using a non-parametric approach. *Journal of Geophysical Research: Oceans*, *126*(12), e2021JC017946.
Serra-Pompei, C., Soudijn, F., Visser, A. W., Kiørboe, T., & Andersen, K. H. (2020). A general size-and trait-based model of plankton communities. *Progress in Oceanography*, *189*, 102473. doi: 10.1016/j.pocean.2020.102473
Serra-Pompei, C., Ward, B. A., Pinti, J., Visser, A. W., Kiørboe, T., & Andersen, K. H. (2022). Linking plankton size spectra and community composition to carbon export and its efficiency. *Global Biogeochemical Cycles*, e2021GB007275.
Smoluchowski, M. v. (1916). Drei vortrage uber diffusion, brownsche bewegung und koagulation von kolloidteilchen. *Zeitschrift fur Physik*, *17*, 557–585.
Stemmann, L., Eloire, D., Sciandra, A., Jackson, G., Guidi, L., Picheral, M., & Gorsky, G. (2008). Volume distribution for particles between 3.5 to 2000 µm

in the upper 200 m region of the South Pacific Gyre. *Biogeosciences*, *5*(2), 299–310.

Stokes, G. G. (1851). On the effect of the internal friction of fluids on the motion of pendulums. *Transactions of the Cambridge Philosophical Society*, *9*(8).

Suess, E. (1980). Particulate organic carbon flux in the oceans—surface productivity and oxygen utilization. *Nature*, *288*(5788), 260–263. doi: 10.1038/288260a0

Syvitski, J. P., Asprey, K., & Leblanc, K. (1995). In-situ characteristics of particles settling within a deep-water estuary. *Deep Sea Research Part Ii: Topical Studies in Oceanography*, *42*(1), 223–256. doi: 10.1016/0967-0645(95)00013-g

Tappan, H., & Loeblich Jr, A. R. (1973). Evolution of the oceanic plankton. *Earth-Science Reviews*, *9*(3), 207–240. (Publisher: Elsevier)

Toktamış, D., Toktamış, H., & Yazıcı, A. N. (2016). The effects of thermal treatments on the thermoluminescence properties of biogenic minerals present in the seashells. *Radiation Effects and Defects in Solids*, *171*(11-12), 951–964.

Tréguer, P., & Jacques, G. (1992). Review Dynamics of nutrients and phytoplankton, and fluxes of carbon, nitrogen and silicon in the Antarctic Ocean. In *Weddell Sea Ecology* (pp. 149–162). Springer. doi: 10.1007/978-3-642-77595-6_17

Van der Jagt, H., Friese, C., Stuut, J. W., Fischer, G., & Iversen, M. H. (2018). The ballasting effect of Saharan dust deposition on aggregate dynamics and carbon export: Aggregation, settling, and scavenging potential of marine snow. *Limnology and Oceanography*, *63*(3), 1386–1394. doi: 10.1002/lno.10779

Visser, A. W., & Jónasdóttir, S. H. (1999). Lipids, buoyancy and the seasonal vertical migration of Calanus finmarchicus. *Fisheries Oceanography*, *8*, 100–106.

White, F. M. (1991). *Viscous Fluid Flow.* New York, NY: McGraw-Hill.

Wiesner, M. R. (1992). Kinetics of aggregate formation in rapid mix. *Water Research*, *26*(3), 379–387. doi: 10.1016/0043-1354(92)90035-3

Table 1. Estimated exponent $b \quad \pm \quad s$ for excess density vrs aggregate size power law where s is the 95% confidence interval. Δ_r is the $\log_{10} r$ range of aggregate size, and n the number of observations. References as given, and indicate field or lab studies.

b	$\pm s$	Δ_r	n		*reference*	
-0.38	1.21	0.5	14		(Alldredge & Gotschalk, 1989)	Field
-1.49	0.15	1.9	76		(Alldredge & Gotschalk, 1988)	Field
-2.09	1.22	0.5	13	i	(Azetsu-Scott & Johnson, 1992)	Field
-1.09	1.88	0.4	15	ii	–´´–	Lab
-0.72	0.20	0.8	37		(Iversen et al., 2010)	Field
-0.83	0.55	0.9	104		(Belcher et al., 2016)	Field
-1.11	0.94	0.8	10		(Carder et al., 1982)	Field
-2.18	0.28	1.0	332		(Diercks & Asper, 1997)	Field
-1.07	0.09	1.2	294		(Engel & Schartau, 1999)	Lab
-1.21	0.05	1.1	20		(Gibbs, 1985)	Field
-1.46	0.05	1.6	1224		Chase 1979	Field
-1.13	0.14	1.1	63	i	(Iversen & Ploug, 2010)	Lab
-1.20	0.12	0.8	26	ii	–´´–	Lab
-1.01	0.20	0.5	97	iii	–´´–	Lab
-0.46	0.30	0.5	99		(Hill et al., 1998)	Field
-0.51	0.23	0.9	187		(Iversen & Ploug, 2013)	Lab
-1.34	0.26	1.1	153		(Iversen & Robert, 2015)	Lab
-1.37	0.20	1.4	54		(Kajihara, 1971)	Field
-2.12	0.59	0.8	61	i	(Laurenceau-Cornec et al., 2015)	Field
-1.24	0.21	0.8	59	ii	–´´–	Lab
-1.24	0.21	0.8	72	i	(Laurenceau-Cornec et al., 2020)	Lab
-0.35	0.19	0.7	131	ii	–´´–	Lab
-1.53	0.12	1.2	274	i	(Engel et al., 2009)	Lab
-1.07	0.09	1.2	249	ii	–´´–	Lab
-0.74	0.14	1.2	296	iii	–´´–	Field
-1.53	0.70	0.9	49		(Nowald et al., 2009)	Field
-1.22	0.12	1.7	149		(Syvitski et al., 1995)	Field
-0.95	0.37	1.3	57	i	(Van der Jagt et al., 2018)	Field
-2.01	0.30	1.2	85	ii	–´´–	Field
-0.88	0.23	1.9	36		(Guidi et al., 2008)	Field
-1.65	0.26	1.7	41		(McDonnell & Buesseler, 2010)	Field
-2.24	0.78	1.0	28		(Jouandet et al., 2011)	Field
-1.59	0.02	1.2	1654		(Bach et al., 2019)	Field
-0.11	0.25	0.7	36		(Gärdes et al., 2011)	Lab
-1.74	0.27	1.4	154		(Iversen & Lampitt, 2020)	Field
-1.38	0.02	4.0	6332		All data points	-